

Discovery and Characteristics of the Rapidly Rotating Active Asteroid (62412) 2000 SY178 in the Main Belt

Scott S. Sheppard¹ and Chadwick Trujillo²

ABSTRACT

We report a new active asteroid in the main belt of asteroids between Mars and Jupiter. Object (62412) 2000 SY178 exhibited a tail in images collected during our survey for objects beyond the Kuiper Belt using the Dark Energy Camera (DECam) on the CTIO 4 meter telescope. We obtained broad-band colors of 62412 at the Magellan telescope, which along with 62412's low albedo suggest it is a C-type asteroid. 62412's orbital dynamics and color strongly correlate with the Hygiea family in the outer main belt, making it the first active asteroid known in this heavily populated family. We also find 62412 to have a very short rotation period of 3.33 ± 0.01 hours from a double-peaked light curve with a maximum peak-to-peak amplitude of 0.45 ± 0.01 magnitudes. We identify 62412 as the fastest known rotator of the Hygiea family and the nearby Themis family of similar composition, which contains several known main belt comets. The activity on 62412 was seen over 1 year after perihelion passage in its 5.6 year orbit. 62412 has the highest perihelion and one of the most circular orbits known for any active asteroid. The observed activity is probably linked to 62412's rapid rotation, which is near the critical period for break-up. The fast spin rate may also change the shape and shift material around 62412's surface, possibly exposing buried ice. Assuming 62412 is a strengthless rubble pile, we find the density of 62412 to be around 2200 kg m^{-3} .

Subject headings: Kuiper belt: general – Oort Cloud – comets: general – minor planets, asteroids: general – planets and satellites: formation

1. Introduction

Comets are generally defined as objects that display dust and/or gas emitting from their surfaces. Observationally, this means detecting either a coma or tail from the object. The

¹Department of Terrestrial Magnetism, Carnegie Institution for Science, 5241 Broad Branch Rd. NW, Washington, DC 20015, USA, ssheppard@carnegiescience.edu

²Gemini Observatory, 670 North A'ohoku Place, Hilo, HI 96720, USA

main source of the observed activity in most comets is likely the sublimation of water ice. Comets are traditionally thought to originate in the Kuiper Belt as short-period comets or in the Oort cloud as long-period comets. Some comets could also originate in the Trojan regions of the giant planets, but no definitive examples are known. Elst et al. (1996) reported activity around a main belt asteroid now called 133P/Elst-Pizarro. Hsieh and Jewitt (2006) detailed the observed activity around a few main belt asteroids between Mars and Jupiter. Hsieh and Jewitt (2006) coined these objects Main Belt Comets (MBCs) as it was thought that Main Belt Asteroids (MBAs) would not be able to sustain any observable activity since water ice should be unstable on their surfaces. There are now at least 12 known objects well within the main asteroid belt that have shown significant activity over the past several years. The source of this activity may be different for the various objects and could include ice sublimation, impact ejecta or rotational breakup (Jewitt 2012; Capria et al. 2012). Because the source of the observed activity in these main belt objects may be unrelated to cometary ice sublimation, these objects are now collectively called active asteroids. The main belt comets are a subset of the active asteroids in which water ice is thought to be the source of the activity observed for the objects. It is important to determine whether the observed activity in an asteroid is driven by volatile inventory or not as ices are important for understanding the chemistry of the early solar nebula and planet formation (Castillo-Rogez and Schmidt 2010; Schmidt and Castillo-Rogez 2012).

Impacts have been inferred for a few active asteroids, such as (596) Scheila and P/2012 F5 (Gibbs), because of the large brightening and quick fading indicative of an impulsive event like an impact (Jewitt et al. 2010, 2011; Snodgrass et al. 2010; Ishiguro et al. 2011; Hsieh et al. 2012; Hainaut et al. 2012; Kim et al. 2012; Stevenson et al. 2012; Moreno et al. 2012; Kleyana et al. 2013; Agarwal et al. 2013). Ice sublimation is inferred for some active asteroids, such as 133P and 238P, because of repeated and prolonged activity only seen near the perihelion of the objects (Hsieh et al. 2010,2011). Newly discovered active asteroid P/2014 S4 (Gibbs) near the outer main belt EOS family complex could also be from water ice sublimation as activity was first seen near perihelion, very similar to the nearby MBC P/2012 T1 (PanSTARRS) (Gibbs et al. 2014; Hsieh et al. 2013). Though water ice is unstable at the surface of an MBA, it could survive a few meters below the surface for billions of years (Schorghofer 2008; Prialnik and Rosenberg 2009). To date, no direct or spectroscopic ice detection has been made for an active asteroid, but this is not unexpected because of the estimated low activity and low active surface areas of these objects (Hsieh et al. 2011; O’Rourke et al. 2013; Jewitt et al. 2014).

The known active asteroids are unlikely to have recently arrived at their locations but have been within the main asteroid belt for billions of years. Thus these objects are not dynamically related to the current short or long period comet populations (Levison et al.

2006; Haghhighipour 2009). It is thought that these asteroids likely formed near their present locations but it is possible some could have originated in the outer solar system and become captured in their current orbits very early in the solar system’s history during the planetary migration era (Levison et al. 2009; Walsh et al. 2011,2012). It is of interest to know whether the active asteroids formed near their present locations or were captured from the outer solar system as any volatile content within them may have played an important role in the formation of the terrestrial planets, including water delivery to Earth (Mottl et al. 2007; O’Brien et al. 2014).

We have discovered a new active asteroid in the outer main belt of asteroids. (62412) 2000 SY178 joins the other twelve objects known to show activity in the main belt and thus can help us further understand these unusual objects. We obtained detailed follow-up observations of 62412 after the initially observed activity from the object.

2. Observations

The main belt asteroid (62412) 2000 SY178 was serendipitously imaged three times on UT March 28, 2014 at the CTIO 4m telescope with the Dark Energy Camera (DECam) during our ongoing survey to find objects beyond the Kuiper Belt (see Trujillo and Sheppard (2014) for details of the survey). DECam is a wide-field optical imager that covers about 2.7 square degrees per image using sixty-two 2048×4096 CCD chips. The pixel scale is 0.263 arcseconds per pixel. Activity was seen on three DECam images of 330 to 420 seconds taken using the very wide VR filter with seeing at about 1 arcsecond Full Width at Half Maximum (FWHM). The faint tail was observed at a position angle of 295 ± 2 degrees extending about 1 arcminute from the nucleus of 62412.

Follow-up observations of 62412 were obtained with the IMACS camera on the 6.5 meter Magellan-Baade telescope on UT May 1 and 2, 2014 (Table 1). IMACS has 8 CCD chips of 2048×4096 with a pixel scale of 0.20 arcseconds per pixel. Standard image reduction techniques were used including bias subtraction and flat-fielding from dithered twilight images. A clear tail for 62412 was evident at a position angle of 297 ± 2 degrees and extending about one arcminute from the object in six 420 second images in the VR filter (Figure 1). There was no evident anti-tail on the opposite side of the main tail of the object. The width of the tail is similar to the FWHM of the images suggesting it is not resolved. Once it was confirmed that 62412 was an active asteroid it was routinely observed using 30 second exposures over about an 8 hour time span on May 2, 2014 in 0.8 arcsecond seeing (Table 2). Most of these observations were taken in the r’-band to look for variability, but some were obtained in the g’, i’ and z’-bands to measure the color of the surface of the object. There

is no obvious coma with only a faint tail observed near 62412 and thus the photometry of the nucleus should not be significantly contaminated (Figure 2). We used an aperture of radius 3 arcseconds for photometry and the Sloan standard star field around DLS-1359 for photometric calibration.

Four 200 second images of 62412 in the VR filter were obtained on UT August 29, 2014 at the 8.2 meter Subaru telescope on Mauna Kea in Hawaii. The Suprime-Cam imager was used with a pixel scale of 0.20 arcseconds per pixel in 0.7 arcsecond seeing. No coma or tail was evident around 62412, suggesting the activity slowed or is no longer present. We also found 62412 at two epochs on archived images from the MegaCam imager on the Canada-France-Hawaii Telescope (CFHT) using the Solar System Object Image Search tool (SSOS) (Gwyn et al. 2012). MegaCam has a pixel scale of 0.187 arcseconds per pixel. On UT January 25, 2012 the main image was a 384 second exposure in the r-band. 62412 was easily detected but no obvious coma or tail was seen in 1.1 arcsecond seeing, indicating the object was not active. On UT January 4, 2013 several i-band exposures of 560 seconds each were obtained with 62412 in the field. No visible coma or tail was observed in 0.8 arcsecond seeing in any of the i-band images, suggesting just before perihelion the object had yet to become active.

3. Results and Analysis

3.1. Orbit

Newly identified active asteroid 62412 has been observed without activity identification for over 15 years and thus has a well-determined orbit in the outer main belt of asteroids (Table 3). 62412 has a Tisserand parameter of 3.20, which is larger than 3 as is typical for main belt asteroids but not short-period comets (Fernandez et al. 2002). Several previous active asteroids in the outer main belt have been identified within the Themis family, but 62412’s current inclination is too high for this association (Figure 3). In order to determine the proper orbital elements of 62412 and look for family membership, we numerically integrated its orbit under the influence of the planets using the Mercury program (Chambers 1999). We found the orbit of 62412 to be stable for the age of the solar system with its proper orbital elements shown in Table 3.

62412’s proper inclination puts the object within the highly populated Hygiea family (Masiero et al. 2013; Carruba 2013; Milani et al. 2014). The Hygiea family is named after 10 Hygiea, which is a C-type asteroid and likely the parent body of most of the family members in this region (Parker et al. 2008; Carruba et al. 2014). This is the first known active

asteroid within the Hygiea family. The Hygiea family is likely very old with an age of about 2 to 3 billion years (Nesvorny et al. 2005; Carruba et al. 2014).

62412 passed perihelion on UT March 21, 2013 and currently has about a 5.6 year orbital period. Thus the tail was first seen about 1 year after perihelion, which is consistent with ice sublimation after some thermal lag from warming near perihelion. However, 62412 currently has one of the lowest eccentricities and the highest perihelia of the known active asteroids (Figures 4 and 5). These orbital parameters call into question ice sublimation caused by 62412’s recent perihelion passage especially compared to some other active asteroids with closer and more eccentric orbits. Because of the faintness of the tail, it is currently unknown when the tail first appeared, but it wasn’t obvious in images leading up to perihelion and appears to have faded from detection later in its orbit from our second round of follow-up observations in late August 2014 (Table 1). Further monitoring of 62412 is encouraged to help observe when and how the activity arises in order to determine the cause of the activity.

3.2. Colors, Albedo and Size

The WISE survey serendipitously observed 62412 in May 2010 when the object was near aphelion (Masiero et al. 2011). Masiero et al. (2011) found an effective radius of 5.187 ± 0.171 and optical albedo of 0.0653 ± 0.0097 for 62412 using an H magnitude of 13.5. This makes 62412 the second largest known active asteroid (Bauer et al. 2012). The largest active asteroid, (596) Scheila, is believed to have activity caused by a recent impact event (Ishiguro et al. 2011; Jewitt et al. 2011; Moreno et al. 2011a; Hsieh et al. 2012; Bodewits et al. 2014).

The optical colors of 62412 show it to have a fairly flat spectral slope (Table 4 and Figure 6). This flat slope along with the negative principal component color value found using the g' , r' , and i' photometry as defined by Ivezić et al. (2001) and the $i'-z'$ color are consistent with a C-type asteroid (Parker et al. 2008). The color of 62412 correlates well with the Hygiea family as the family is composed of mostly C-type objects (Parker et al. 2008; Carvano et al. 2010; Carruba et al. 2014). The low albedo found by Masiero et al. (2011) for 62412 also suggests it is a C-type asteroid (Mainzer et al. 2012; 2011). These are similar characteristics to the outer main belt MBCs such as 238P (Read) and 133P (Hsieh et al. 2004,2009).

The reduced magnitude $M_R(1, 1, 0)$ of 13.82 ± 0.23 determined for 62412 during our UT May 2, 2014 observations would be 14.18 ± 0.25 mags in the V-band, which makes the object fainter than the assumed 13.5 mag absolute magnitude used by Masiero et al. (2011) in the

WISE albedo observations. The exact absolute magnitude depends on the unknown phase function of 62412. We assumed a linear 0.07 mags per degree for the phase function based on the average of the C-type asteroids phase curves at low phase angles (Schaefer et al. 2010). Regardless, 62412 does not currently appear to be anomalously bright, which suggests there is little to no coma around the object and thus photometry should be mostly of the nucleus as shown in Figure 2.

The effective radius of an object can be calculated using the relation $M_R(1, 1, 0) = m_{\odot} - 2.5 \log [p_R r_e^2 / 2.25 \times 10^{16}]$ where m_{\odot} is the apparent red magnitude of the sun (-27.07 : Hartmann et al. 1990), p_R is the red geometric albedo and r_e (km) is the effective circular radius of the object. Using the WISE albedo of 0.0653 we get an effective radius of 3.9 ± 0.3 km, which is smaller than found by Masiero et al. (2011) but consistent with our fainter absolute magnitude.

3.3. Rotation

We used the Phase Dispersion Minimization (PDM) method to determine possible periodicity in the light curve of 62412 (Stellingwerf 1978). In PDM, the metric is the Θ parameter, which is essentially the variance of the unphased data divided by the variance of the data when phased by a given period. The best fit period should have a very small dispersion compared to the unphased data and thus $\Theta \ll 1$ indicates that a good fit has been found.

From Figure 7 it is apparent that a single-peaked period of 1.665 hours and a double-peaked period of 3.33 hours are the best fits to the light curve of 62412. When phasing the data together (Figure 8) it is obvious that the double-peaked period is the best fit as the two minimum peaks have different amplitudes. A double-peaked periodic light curve is produced when an elongated object's effective radius to our line of sight changes as the object rotates. That is, the projected cross section of an object would go between two minima (short axis) and two maxima (long axis) during one complete rotation. A single-peaked light curve is likely caused by albedo or surface variations.

Thus we find a double-peaked period of 3.33 ± 0.01 hours with a maximum peak-to-peak amplitude of 0.45 ± 0.01 magnitudes for 62412. The two brightest peaks, which are when the two opposite sides of maximum surface area of the object are visible, appear to be similar. The two fainter peaks of the light curve are different by about 0.05 magnitudes, showing the object has an elongated irregular shape.

62412 is small enough that its spin is not likely primordial and thus has been modified

over the age of the solar system (Steinberg and Sari 2014). The large size and distant orbit of 62412 make it less sensitive to the YORP spin-up effect than the other mostly smaller active asteroids (Nesvorný and Vokrouhlický 2007; Marzari et al. 2011; Jacobson et al. 2014). The size of 62412 is very near the transition radius where YORP is expected to significantly modify the spins of asteroids (Bottke et al. 2002; Pravec et al. 2002; Carbognani 2011; Steinberg and Sari 2011). Thus the short rotation period of 62412 could be from the YORP effect, but if not from YORP, an impact and/or sublimation of ice off the surface could have initially spun up 62412 to the state it is now (Wiegert 2014; Polishook 2014).

3.4. Shape, Critical Period and Density

For an object that is elongated, the peak-to-peak amplitude of the rotational light curve allows for the determination of the projection of the body shape into the plane of the sky. Assuming we are viewing the object equatorially, the lower limit on the a to b axis ratio is $a/b = 10^{0.4\Delta m}$ (Binzel et al. 1989), where $a \geq b \geq c$ are the semi-axes with the object in rotation about the c axis and Δm is expressed in magnitudes. If the light curve amplitude of 62412 is caused by an elongated shape, 62412 has $a/b \geq 1.51$. Using the effective radius of 3.9 km found earlier, we get $a \sim 4.8$ km and $b \sim 3.2$ km.

An object will be near breakup if it has a rotation period near the critical rotation period (P_{crit}) at which centripetal acceleration equals gravitational acceleration towards the center of a rotating spherical object,

$$P_{crit} = \left(\frac{3\pi}{G\rho} \right)^{1/2} \quad (1)$$

where G is the gravitational constant and ρ is the density of the object. With $\rho = 2000$ kg m⁻³, which is on the high end of C-types but about the density of 10 Hygiea and Ceres (Baer et al. 2011; Carry 2012), the critical period is about 2.3 hours. At shorter periods the object may break apart while slightly longer periods the equilibrium figures are triaxial ellipsoids which are elongated from the large centripetal force (Weidenschilling 1981; Holsapple 2001).

For an elongated strengthless object, the critical period of break-up will happen at a slower spin period (Samarasinha et al. 2004, Jewitt 2012):

$$P_{crit} = a/b \left(\frac{3\pi}{G\rho} \right)^{1/2} \quad (2)$$

For 62412, $a/b \geq 1.51$ and thus $P_{crit} \geq 3.5$ hours for a density of 2000 kg m⁻³. Thus 62412's period appears to be faster than the critical period for break-up and thus the object should

be unstable to rotational fission, especially if its density is less than 2000 kg m^{-3} , as expected for most C-type asteroids (Mainzer et al. 2012). Holsapple (2004) found that the spin period for instability should be even slower than the simple discussion above, making it even more likely that 62412 is spinning faster than the critical period, though unknown cohesive forces will be important (Richardson et al. 2009; Chang et al. 2014; Rozitis et al. 2014).

Assuming 62412 is at P_{crit} and is a strengthless rubble pile, we find from Equation 2 that the density would be about 2200 kg m^{-3} , which is significantly greater than expected for comets (Thomas et al. 2013) and slightly greater than expected for C-type asteroids of 62412’s size (Baer et al. 2011, Carry 2012).

4. Discussion

4.1. Cause of 62412’s Tail

Above we show that 62412 is likely spinning near or faster than its critical speed for breakup. This strongly suggests that the tail observed for 62412 is in part created by its rapid rotation. The observed tail is aligned with the negative velocity vector, which usually means relatively large particles in the orbital plane (Finson and Probst 1968; Lisse et al. 2004; Hsieh et al. 2004; Moreno et al. 2011b). These large particles could be the remnants of an earlier outburst or slow moving ejected material from 62412’s rapid rotation (see Jewitt et al. 2010; Snodgrass et al. 2010).

Some of the active asteroids appear to show activity within a few months of perihelion, which has been attributed to water ice sublimation (Hsieh et al. 2010,2011,2013). For 62412 the first detection of activity was in early 2014, over a year after perihelion (Figure 9). 62412 showed no activity leading up to and just before perihelion in early 2013 from deep images similar to ours that were serendipitously obtained at the CFHT telescope during this time. Thus the activity likely started or occurred around perihelion or afterwards. It is possible that 62412 has a high thermal inertia since it was not active just before perihelion but is active well beyond perihelion, suggesting heat took awhile to penetrate to depth where ice could be.

The short rotation period may or may not be directly ejecting material off the surface of 62412, but it has likely changed the shape and is shifting or has shifted material around the object (Bottke et al. 2002; Richardson et al. 2005; Minton 2008; Statler 2009; Harris et al. 2009; Scheeres 2009; Holsapple 2010; Walsh et al. 2012; Cotto-Figueroa et al. 2013; Richardson and Bowling 2014). If ices are contained within 62412, this shifting of material could expose fresh ice to the surface, which could then sublimate away dragging material

with it. The changing shape and shifting of material from the rapid rotation may be an ongoing process that could constantly expose new ice. 62412 is a good candidate to have ice buried just under its surface since it is relatively large and the parent body 10 Hygiea was recently shown to have a 3 micron spectral feature indicative of water ice (Takir and Emery 2012).

Our last observations of 62412 in late August 2014 found no obvious tail near the object. Further monitoring of 62412 is necessary to better determine the cause of its activity. If the activity is seen sporadically throughout 62412’s orbit, fissioning of material off the surface is most likely. If the activity only appears near or just after perihelion, ice sublimation would be the most likely cause, though helped by the short rotation period. If no further activity is observed, it is possible 62412 experienced a recent impact that lifted material from the surface.

4.2. Comparison to Other Active Asteroids and Comets

Rapid rotation has been suggested as the cause for the multiple tail features observed for active asteroid P/2013 P5 PanSTARRS, though no rotation period has been measured to confirm this (Jewitt et al. 2013; Hainaut et al. 2014; Moreno et al. 2014). Active asteroids P/2012 A2 LINEAR and P/2013 R3 Catalina-PanSTARRS have also been suggested as possible rotationally unstable objects, though again, no rotation periods are known for these objects and impact generated activity is a more likely scenario for P/2012 A2 LINEAR (Jewitt et al. 2010, 2011; Snodgrass et al. 2010; Hainaut et al. 2012; Hirabayashi et al. 2014). Asteroid pairs, which are asteroids not bound to each other but on very similar orbits with very similar colors could also have formed from rotational-fission or impacts (Vokrouhlicky and Nesvorny 2008; Pravec and Vokrouhlicky 2009; Pravec et al. 2010; Jacobson and Scheeres 2011; Moskovitz 2012; Jacobson et al. 2014; Wolters et al. 2014; Polishook et al. 2014).

The Themis family member active asteroid 133P has a period of 3.471 hours with an axis ratio greater than 1.45 (Hsieh et al. 2004), which are characteristics similar to 62412. There is no obvious coma around 62412 or 133P, indicating extremely low ejection velocities for dust particles (Jewitt et al. 2014). Both 62412 and 133P are very fast rotators compared to known comets (Jorda and Gutierrez 2000; Samarasinha et al. 2004), and because of their aspherical shapes, are likely near or faster than the critical rotational speed for breakup. Jewitt et al. (2014) suggest the high centripetal acceleration from 133P’s rapidly rotating nucleus aids in the escape of near-surface water ice and dust from the object.

Using data from the updated Asteroid Lightcurve Data Base (LCDB: Warner et al.

2009), Figure 10 shows that 62412 has the fastest known rotation speed of any object in the mostly C-type Hygiea and Themis families. Active asteroid 133P has the next fastest known rotation of any of these objects. This strongly suggests that these short rotation periods are an important part of the activity seen in these objects. In fact, 62412 is the only object in these two families that requires a density greater than 2000 kg m^{-3} in order to be stable (Figure 11). Figure 11 also shows that asteroid (656) Beagle is likely near the critical period for fission, which is interesting because Beagle is the largest member of the young $\sim 10 \text{ Myr}$ sub-family in the much older Themis population (Nesvorný et al. 2008).

62412 has a much higher density than any known short or long period comet. The short and long period comets appear to have densities closer to 1000 kg m^{-3} , which is thought to be because of their more distant formation in the ice rich outer solar system (Weissman et al. 2004). The C-type asteroids probably consist of much more rock giving them a density closer to 2000 kg m^{-3} (Baer et al. 2011, Carry 2012). Thus 62412 likely formed in a much different location than the short or long period comets.

4.3. Number of Active Asteroids

We have observed about 700 square degrees of sky to deeper than 24th magnitude during our ongoing survey for objects beyond the Kuiper Belt edge (Trujillo and Sheppard 2014). The survey has generally been between 5 and 20 degrees from the ecliptic. Because of the depth and large area, our survey has an unprecedented ability to see faint coma and tails around objects that other surveys would not detect. This increased sensitivity means we can detect lower activity active asteroids, which are also likely to be older as activity is expected to decrease over time. Though we would only detect the coma and/or tail of an active object by serendipitous visual inspection, it is generally obvious to identify activity while looking through the survey images. We have looked at all survey images visually while searching for distant solar system objects. In this way we not only observed a tail to 62412 but also discovered comet C/2014 F3 Sheppard-Trujillo as well as detected many known comets (Sheppard and Trujillo 2014). The faint tail of 62412 was not detected by any other survey even though it was within several automated surveys fields of view and has been imaged many times in the last fifteen years.

In this crude way, we can put order of magnitude constraints on the number of possible active asteroids in the main belt of asteroids. We detected about 15,000 MBAs and one active asteroid. This detection rate gives a ratio of active asteroid to MBA of 1:15,000. Thus with about 1 to 2 million main belt asteroids larger than 1 km predicted (Tedesco et al. 2005), we would expect about 100 active asteroids, which is consistent with earlier

estimates (Hsieh 2009).

The Hygiea family likely has about 10,000 members larger than 1 km (Tedesco et al. 2005) and thus we should only expect one as an active asteroid. The Themis family is a hundred times larger and thus we would expect this family to have the majority of the active asteroids, in which it appears this is the case as three to five of the known active asteroids out of thirteen total are near the Themis family (Figure 3). This of course assumes all asteroids are just as likely to become active. In reality the spin state, collisional environment, surface properties and volatile content of the asteroids are very important factors in determining what objects become active. This should favor more MBCs in the outer belt as they are the most likely to have retained water ice over the age of the solar system as shown by the recent possible detections of water ice on Ceres, Themis and Cybele (Rivkin and Emery 2010, Campins et al. 2010; Licandro et al. 2011; Kuppers et al. 2014).

5. Summary

We report the 13th known active asteroid in the main asteroid belt, (62412) 2000 SY178. There is no obvious coma around the object but it exhibits a faint tail. 62412 is about 4 km in radius, making it the second largest known active asteroid. The main results of this paper are:

1) The orbit of 62412 is stable for the age of the solar system and has a Tisserand parameter greater than 3, which is typical of main belt asteroids. We determine that proper orbital elements for 62412 make it the first known active asteroid in the Hygiea family in the outer belt of asteroids.

2) The optical colors of 62412 match those of typical primitive C-type asteroids, which is the dominate type of asteroid in the Hygiea family.

3) 62412 has the highest perihelion and one of the lowest eccentricities of the known active asteroids. The observed tail was first seen over 13 months after perihelion with no activity observed just before perihelion.

4) We find a rapid rotation of 3.33 ± 0.01 hours for 62412. The double-peaked peak-to-peak light curve amplitude of 0.45 ± 0.01 magnitudes suggests 62412 is an elongated object with an a to b axial ratio greater than or equal to 1.51.

5) 62412 is likely rotating faster than the critical period for rotational breakup of a strengthless body. To prevent rotational fission, it must have a density of about 2200 kg m^{-3} . This is on the high end for C-type asteroids and well above known short and long

period comet densities.

6) 62412 has the fastest spin rate of any known member of the Hygiea or Themis asteroid families as well as any long or short period comet. This suggests the spin state may be the cause or is at least a major factor in the observed activity. The rapid rotation may allow particles to directly escape from the surface and likely causes changes in the shape and shifts material around on 62412, which could expose possible buried ices.

7) The number of active asteroids in the main belt is likely to be around 100 objects, consistent with previous estimates.

Acknowledgments

This project used data obtained with the Dark Energy Camera (DECam), which was constructed by the Dark Energy Survey (DES) collaborating institutions: Argonne National Lab, University of California Santa Cruz, University of Cambridge, Centro de Investigaciones Energeticas, Medioambientales y Tecnologicas-Madrid, University of Chicago, University College London, DES-Brazil consortium, University of Edinburgh, ETH-Zurich, University of Illinois at Urbana-Champaign, Institut de Ciencies de l’Espai, Institut de Fisica d’Altes Energies, Lawrence Berkeley National Lab, Ludwig-Maximilians Universitat, University of Michigan, National Optical Astronomy Observatory, University of Nottingham, Ohio State University, University of Pennsylvania, University of Portsmouth, SLAC National Lab, Stanford University, University of Sussex, and Texas A&M University. Funding for DES, including DECam, has been provided by the U.S. Department of Energy, National Science Foundation, Ministry of Education and Science (Spain), Science and Technology Facilities Council (UK), Higher Education Funding Council (England), National Center for Supercomputing Applications, Kavli Institute for Cosmological Physics, Financiadora de Estudos e Projetos, Fundacao Carlos Chagas Filho de Amparo a Pesquisa, Conselho Nacional de Desenvolvimento Cientifico e Tecnologico and the Ministerio da Ciencia e Tecnologia (Brazil), the German Research Foundation-sponsored cluster of excellence “Origin and Structure of the Universe” and the DES collaborating institutions. Observations were partly obtained at Cerro Tololo Inter-American Observatory, National Optical Astronomy Observatory, which are operated by the Association of Universities for Research in Astronomy, under contract with the National Science Foundation. C.T. is supported by the Gemini observatory, which is operated by the Association of Universities for Research in Astronomy, Inc., on behalf of the international Gemini partnership of Argentina, Australia, Brazil, Canada, Chile, the United Kingdom, and the United States of America. This research used the facilities of the Canadian Astronomy Data Centre operated by the National Research Council of Canada

with the support of the Canadian Space Agency. We thank H. Hsieh for comments on this manuscript. This paper includes data gathered with the 6.5 meter Magellan Telescopes located at Las Campanas Observatory, Chile. This research was funded by NASA Planetary Astronomy grant NNX12AG26G.

REFERENCES

- Agarwal, J., Jewitt, D., and Weaver, H. 2013, *ApJ*, 769, 46.
- Baer, J., Chesley, S., and Matson, R. 2011, *AJ*, 141, 143.
- Bauer, J. et al. 2012, *ApJ*, 747, 49.
- Bodewits, D., Vincent, J. and Kelley, M. 2014, *Icarus*, 229, 190.
- Bottke, W., Vokrouhlicky, D., Rubincam, D. and Broz, M. 2002, in *Asteroids III*, ed. W. Bottke, A. Cellino, P. Paolicchi, and R. Binzel (Tucson: Univ. of Arizona Press), 395.
- Campins, H. et al. 2010, *Nature*, 464, 1320.
- Capria, M., Marchi, S., De Sanctis, M., Coradini, A. and Ammannito, E. 2012, *AA*, 537, 71.
- Carbognani, A. 2011, *Icarus*, 211, 519.
- Carruba, V. 2013, *MNRAS*, 431, 3557.
- Carruba, V., Domingos, R., Huaman, M., dos Santos, C., and Souami, D. 2014, *MNRAS*, 437, 2279.
- Carry, B. 2012, *PSS*, 73, 98.
- Carvano, J., Hasselmann, P., Lazzaro, D., and Mothe-Diniz, T. 2010, *AA*, 510, 43.
- Castillo-Rogez, J. and Schmidt, B. 2010, *GeoPhysical Research Letters*, 37, 10202.
- Chambers, J. 1999, *MNRAS*, 304, 793.
- Chang, C., Waszczak, A., Lin, H., Ip, W., Prince, T., Kulkarni, S., Laher, R. and Surace, J. 2014, *ApJ Letters*, 791, L35.
- Cotto-Figueroa, D., Statler, T., Richardson, D. and Tanga, P. 2013, *BAAS*, 45, 106.09.
- Elst, E., Pizarro, O., Pollas, C. et al. 1996, *IAUC Circ.*, 6496, 1.
- Fernandez, J., Gallardo, T. and Brunini, A., 2002, *Icarus*, 159, 358.
- Finson, M. and Probst, R. 1968, *ApJ*, 154, 327.
- Gibbs, A., Sato, H. and Williams, G. 2014, *CBET* 3991: 20140927.
- Gwyn, S., Hill, N., and Kavelaars, J., 2012, *PASP*, 124, 579.

- Haghighipour, N. 2009, *Meteoritics and Planetary Science*, 44, 1863.
- Hainaut, O. et al. 2012, *AA*, 537, 69.
- Hainaut, O., et al. 2014, *AA*, 563, 75.
- Harris, A., Fahnestock, E., and Pravec, P. 2009, 199, 310.
- Hartmann, W., Tholen, D., Meech, K. and Cruikshank, D. 1990, *Icarus*, 83, 1.
- Hirabayashi, M., Scheeres, D., Sanchez, D., and Gabriel, T. 2014, *ApJ Letters*, 789, L12.
- Holsapple, K. 2001, *Icarus*, 154, 432.
- Holsapple, K. 2004, *Icarus*, 172, 272.
- Holsapple, K. 2010, *Icarus*, 205, 430.
- Hsieh, H., Jewitt, D. and Fernandez, Y. 2004, *AJ*, 127, 2997.
- Hsieh, H. and Jewitt, D. 2006, *Science*, 312, 561.
- Hsieh, H. 2009, *AA*, 505, 1297.
- Hsieh, H., Jewitt, D., Ishiguro, H. 2009, *AJ*, 137, 157.
- Hsieh, H., Jewitt, D., Lacerda, P., Lowry, S., and Snodgrass, C. 2010, *MNRAS*, 403, 363.
- Hsieh, H. et al. 2011, *ApJ*, 736, L18.
- Hsieh, H., Yang, B. and Haghighipour, N. 2012, *ApJ*, 744, 9.
- Hsieh, H. et al. 2013, *ApJ*, 771, L1.
- Ivezic, Z. et al. 2001, *AJ*, 122, 2749.
- Ishiguro, M., et al. 2011, *ApJ*, 740, L11.
- Jacobson, S. and Scheeres, D. 2011, *Icarus*, 214, 161.
- Jacobson, S., Marzari, F., Rossi, A., Scheeres, D. and Davis, D., 2014, *MNRAS*, 439, 95.
- Jewitt, D., Weaver, H., Agarwal, J., Mutchler, M. and Drahus, M., 2010, *Nature*, 467, 817.
- Jewitt, D., Weaver, H., Mutchler, M., Larson, S. and Agarwal, J. 2011, *ApJ*, 733, 4.
- Jewitt, D. 2012, *AJ*, 143, 66.
- Jewitt, D., Agarwal, J., Weaver, H., Mutchler, M., and Larson, S. 2013, *ApJ*, 778, L21.
- Jewitt, D., Ishiguro, M., Weaver, H., Agarwal, J., Mutchler, M. and Larson, S. 2014, *AJ*, 147, 117.
- Jorda, L. and Gutierrez, P. 2000, *EMP*, 89, 135.
- Kim, J., Ishiguro, M., Hanayama, H. et al. 2012, *ApJ*, 746, L11.

- Kleyna, J., Hainaut, O. and Meech, K. 2013, *AA*, 549, 13.
- Kuppers, M. et al. 2014, *Nature*, 505, 525.
- Levison, H., Terrell, D., Wiegert, P., Dones, L., and Duncan, M. 2006, *Icarus*, 182, 161.
- Levison, H., Bottke, W., Gounelle, M., Morbidelli, A., Nesvorny, D., and Tsiganis, K. 2009, *Nature*, 460, 364.
- Licandro, J., Campins, H., Kelley, M., Hargrove, K., Pinilla-Alonso, N., Cruikshank, D., Rivkin, A., and Emery, J. 2011, *AA*, 525, 34.
- Lisse, C., Fernandez, Y., A’Hearn, M. et al. 2004, *Icarus*, 171, 444.
- Mainzer, A. et al. 2011, *ApJ*, 741, 90.
- Mainzer, A. et al. 2012, *ApJ*, 745, 7.
- Marzari, F., Rossi, A., and Scheeres, D. 2011, *Icarus*, 214, 622.
- Masiero, J. et al. 2011, *ApJ*, 741, 68.
- Masiero, J. et al. 2013, *ApJ*, 770, 7.
- Milani, A., Cellino, A., Knezevic, Z., Novakovic, B., Spoto, F. and Paolicchi, P. 2014, *Icarus*, 239, 46.
- Minton, D. 2008, *Icarus*, 195, 698.
- Moreno, F., Licandro, J., Ortiz, J., Lara, L., Ali-Lagoa, V., Vaduvescu, O., Morales, N., Molina, A. and Lin, Z. 2011a, *ApJ*, 738, 130.
- Moreno, F., Lara, L., Licandro, J. et al. 2011b, *ApJ*, 738, L16.
- Moreno, F., Licandro, J., and Cabrera-Lavers, A. 2012, *ApJ*, 761, L12.
- Moreno, F., Licandro, J., Alvarez-Iglesias, C., Cabrera-Lavers, A. and Pozuelos, F. 2014, *ApJ*, 781, 118.
- Moskovitz, N. 2012, *Icarus*, 221, 63.
- Mottl, M., Glazer, B., Kaiser, R., and Meech, K. 2007, *ChEG*, 67, 253.
- Nesvorny, D., Jedicke, R., Whiteley, R., and Ivezić, Z. 2005, *Icarus*, 173, 132.
- Nesvorny, D. and Vokrouhlicky, D. 2007, *AJ*, 134, 1750.
- Nesvorny, D., Bottke, W., Vokrouhlicky, D., Sykes, M., Lien, D. and Stansberry, J. 2008, *ApJ*, 679, L143.
- O’Brien, D., Walsh, K., Morbidelli, A., Raymond, S. and Mandell, A. 2014, *Icarus*, 239, 74.
- O’Rourke, L. et al. 2013, *ApJ*, 774, 13.

- Parker, A., Ivezić, Z., Juric, M., Lupton, R., Sekora, M., and Kowalski, A. 2008, *Icarus*, 198, 138.
- Polishook, D., Moskovitz, N., Binzel, R., DeMeo, F., Vokrouhlicky, D., Zizka, J., and Oszkiewicz, D. 2014, *Icarus*, 233, 9.
- Polishook, D. 2014, *Icarus*, 241, 79.
- Pravec, P., Harris, A. and Michalowski, T. 2002, in *Asteroids III*, ed. W. Bottke, A. Cellino, P. Paolicchi, and R. Binzel (Tucson: Univ. of Arizona Press), 113.
- Pravec, P. and Vokrouhlicky, D. 2009, *Icarus*, 204, 580.
- Pravec, P. et al. 2010, *Nature*, 466, 1085.
- Prialnik, D. and Rosenberg, E. 2009, *AA*, 137, 4313.
- Richardson, D., Elankumaran, P., and Sanderson, R. 2005, *Icarus*, 173, 349.
- Richardson, D., Michel, P., Walsh, K. and Flynn, K. 2009, *PSS*, 57, 183.
- Richardson, J. and Bowling, T. 2014, *Icarus*, 234, 53.
- Rivkin, A. and Emery, J. 2010, *Nature*, 464, 1322.
- Rozitis, B., MacLennan, E. and Emery, J. 2014, *Nature*, 512, 174.
- Samarasinha, N., Mueller, B., Belton, M., and Jorda, L. 2004, in *Comets II*, ed. M. Festou, H. Keller and H. Weaver (Tucson: Univ. of Arizona Press), 281.
- Schaefer, M., Schaefer, B., Rabinowitz, D. and Tourtellotte, S. 2010, *Icarus*, 207, 699.
- Scheeres, D. 2009, *PSS*, 57, 154.
- Schmidt, B. and Castillo-Rogez, J. 2012, *Icarus*, 218, 478.
- Schorghofer, N. 2008, *ApJ*, 682, 697.
- Sheppard, S. and Trujillo, C. 2014, *CBET* 3879
- Smith, J., et al. 2002, *AJ*, 123, 2121.
- Snodgrass, C., Tubiana, C., Vincent, J. et al. 2010, *Nature*, 467, 814.
- Statler, T. 2009, *Icarus*, 202, 502.
- Stellingwerf, R. 1978, *ApJ*, 224, 953.
- Stevenson, R., Kramer, E., Bauer, J., Masiero, J., and Mainzer, A. 2012, *ApJ*, 759, 142.
- Steinberg, E. and Sari, R. 2011, *AJ*, 141, 55.
- Steinberg, E. and Sari, R. 2014, [arXiv:1406.5730](https://arxiv.org/abs/1406.5730)
- Takir, D. and Emery, J. 2012, *Icarus*, 219, 641.

- Tedesco, E., Cellino, A. and Zappala, V. 2005, *AJ*, 129, 2869.
- Thomas, P., et al. 2013, *Icarus*, 222, 550.
- Trujillo, C. and Sheppard, S. 2014, *Nature*, 507, 471.
- Vokrouhlicky, D. and Nesvorny, D. 2008, *AJ*, 136, 280.
- Walsh, K., Morbidelli, A., Raymond, S., O’Brien, D. and Mandell, A. 2011, *Nature*, 475, 206.
- Walsh, K., Morbidelli, A., Raymond, S., O’Brien, D. and Mandell, A. 2012, *Meteoritics and Planetary Science*, 47, 1941.
- Walsh, K., Richardson, D. and Michel, P. 2012, *Icarus*, 220, 514.
- Warner, B., Harris, A. and Pravec, P. 2009, *Icarus*, 202, 134.
- Weidenschilling, S. 1981, *Icarus*, 46, 124.
- Weissman, P., Asphaug, E., and Lowry, S. 2004, in *Comets II*, ed. M. Festou, H. Keller and H. Weaver (Tucson: Univ. of Arizona Press), 337.
- Wolters, S., Weissman, P., Christou, A., Duddy, S., and Lowry, S. 2014, *MNRAS*, 439, 3085.
- Wiegert, P., 2014, arXiv:1407.3714

Table 1. Geometry of the 62412 Observations

UT Date	R (AU)	Δ (AU)	α (deg)	Plane (deg)	True (deg)	PA_{Sun} (deg)	PA_v (deg)	Active
2012 Jan 25.307	3.102	3.028	18.4	-0.64	277.3	68.5	246.3	No
2013 Jan 04.407	2.900	1.950	6.12	-1.69	344.4	271.4	287.6	No
2013 Mar 21	2.892	2.357			Perihelion			
2014 Mar 28.245	3.062	2.144	8.78	1.35	74.4	300.9	291.8	Yes
2014 May 01.192	3.088	2.101	4.44	2.15	80.6	84.9	293.8	Yes
2014 May 02.005	3.089	2.104	4.75	2.16	80.8	87.0	293.9	Yes
2014 Aug 29.246	3.184	3.534	16.2	-0.15	101.8	111.7	291.2	No
2016 Jan 10	3.411	4.332			Aphelion			

Quantities are the heliocentric distance (R), geocentric distance (Δ), phase angle (α), the orbit plane angle which is the angle between the observer and target orbital plane (Plane), true anomaly (True), position angle of the antisolar vector as projected in the plane of the sky (PA_{Sun}), and position angle of the negative velocity vector as projected in the plane of the sky (PA_v). UT Date shows the year, month, and time of day at the start of the observations on each night it was observed. Individual exposure times used for colors and the lightcurve measurements on May 2, 2014 were 30 seconds in the g' , r' , i' and z' filters and they were rotated after each observation to prevent any rotational light curves from influencing the color calculations.

Table 2. r'-band Observations of (62412) 2000 SY178

Airmass	Exp ^b (sec)	UT Date ^c yyyy mm dd.ddddd	Mag. ^d ($m_{r'}$)	Err ^e ($m_{r'}$)
1.239	45	2014 05 01.257820	18.11	0.01
1.247	30	2014 05 01.259440	18.15	0.01
1.524	35	2014 05 02.008044	18.00	0.01
1.436	35	2014 05 02.017719	18.12	0.01
1.424	35	2014 05 02.019155	18.13	0.01
1.413	35	2014 05 02.020601	18.17	0.01
1.335	30	2014 05 02.031678	18.37	0.01
1.326	30	2014 05 02.033055	18.40	0.01
1.318	30	2014 05 02.034398	18.41	0.01
1.221	30	2014 05 02.052500	18.27	0.01
1.215	30	2014 05 02.053842	18.24	0.01
1.209	30	2014 05 02.055208	18.20	0.01
1.146	30	2014 05 02.071504	18.00	0.01
1.142	30	2014 05 02.072858	18.01	0.01
1.137	30	2014 05 02.074213	17.99	0.01
1.087	30	2014 05 02.092905	18.18	0.01
1.084	30	2014 05 02.094259	18.22	0.01
1.081	30	2014 05 02.095613	18.23	0.01
1.052	30	2014 05 02.111794	18.40	0.01
1.050	30	2014 05 02.113160	18.38	0.01
1.048	30	2014 05 02.114525	18.36	0.01
1.031	30	2014 05 02.130683	18.09	0.01
1.030	30	2014 05 02.132049	18.06	0.01
1.029	30	2014 05 02.133437	18.05	0.01
1.024	30	2014 05 02.149190	18.01	0.01
1.024	30	2014 05 02.150544	18.01	0.01
1.024	30	2014 05 02.151910	18.03	0.01
1.027	30	2014 05 02.166215	18.25	0.01
1.028	30	2014 05 02.167593	18.27	0.01
1.029	30	2014 05 02.168958	18.30	0.01

Table 2—Continued

Airmass	Exp ^b (sec)	UT Date ^c yyyy mm dd.ddddd	Mag. ^d ($m_{r'}$)	Err ^e ($m_{r'}$)
1.040	30	2014 05 02.182384	18.45	0.01
1.042	30	2014 05 02.183727	18.43	0.01
1.047	30	2014 05 02.187801	18.29	0.01
1.049	30	2014 05 02.189167	18.26	0.01
1.072	30	2014 05 02.203125	18.04	0.01
1.074	30	2014 05 02.204479	18.02	0.01
1.089	30	2014 05 02.211343	17.98	0.01
1.092	30	2014 05 02.212778	17.98	0.01
1.106	30	2014 05 02.218264	18.01	0.01
1.139	30	2014 05 02.229653	18.14	0.01
1.144	30	2014 05 02.231030	18.15	0.01
1.148	30	2014 05 02.232419	18.18	0.01
1.207	30	2014 05 02.247558	18.40	0.01
1.213	30	2014 05 02.248935	18.39	0.01
1.285	30	2014 05 02.263252	18.18	0.01
1.293	30	2014 05 02.264641	18.16	0.01
1.301	30	2014 05 02.265995	18.14	0.01
1.466	30	2014 05 02.289132	18.00	0.01
1.478	30	2014 05 02.290486	18.02	0.01
1.490	30	2014 05 02.291829	18.03	0.01
1.598	30	2014 05 02.302627	18.20	0.01
1.613	30	2014 05 02.303981	18.25	0.01
1.628	30	2014 05 02.305370	18.26	0.01
1.644	30	2014 05 02.306678	18.29	0.01
1.659	30	2014 05 02.307998	18.31	0.01
1.675	30	2014 05 02.309306	18.34	0.01
1.692	30	2014 05 02.310625	18.38	0.01
1.710	30	2014 05 02.312014	18.39	0.01
1.727	30	2014 05 02.313333	18.42	0.01
1.745	30	2014 05 02.314641	18.43	0.01

Table 2—Continued

Airmass	Exp ^b (sec)	UT Date ^c yyyy mm dd.ddddd	Mag. ^d ($m_{r'}$)	Err ^e ($m_{r'}$)
1.763	30	2014 05 02.315949	18.44	0.01
1.782	30	2014 05 02.317269	18.43	0.01
1.802	30	2014 05 02.318611	18.46	0.01
1.821	30	2014 05 02.319919	18.44	0.01
1.842	30	2014 05 02.321238	18.44	0.01
1.862	30	2014 05 02.322546	18.39	0.01
1.884	30	2014 05 02.323854	18.40	0.01
1.907	30	2014 05 02.325231	18.34	0.01
1.929	30	2014 05 02.326539	18.32	0.01
1.953	30	2014 05 02.327859	18.26	0.01
1.977	30	2014 05 02.329167	18.26	0.01
2.001	30	2014 05 02.330475	18.20	0.01
2.027	30	2014 05 02.331840	18.19	0.01
2.054	30	2014 05 02.333160	18.17	0.01
2.080	30	2014 05 02.334468	18.14	0.01
2.108	30	2014 05 02.335775	18.10	0.01
2.137	30	2014 05 02.337095	18.11	0.01
2.168	30	2014 05 02.338472	18.08	0.01
2.198	30	2014 05 02.339792	18.10	0.01
2.232	30	2014 05 02.341192	18.05	0.01

^bExposure time for the image.

^cDecimal Universal Time at the start of the integration.

^dApparent magnitude in r' filter.

^eUncertainties on the individual photometric measurements.

Table 3. Orbital Information for 62412

Type	a (AU)	e	i (deg)	q (AU)	Q (AU)	P (yr)	T_J
Current	3.151	0.082	4.74	2.892	3.410	5.6	3.20
Proper	3.147	0.114	5.64	2.790	3.506	5.6	3.19

Quantities are the semi-major axis (a), eccentricity (e), inclination (i), perihelion distance (q), aphelion distance (Q), period (P), and Tisserand parameter with respect to Jupiter (T_J). Current orbital elements are from the Minor Planet Center. Proper orbital elements are from our 4.6 billion year numerical integration using the Mercury code (Chambers 1999).

Table 4. Sloan g',r',i',z' Optical Photometry

$m_{r'}$ (mag)	$M_R(1, 1, 0)$	$g'-r'$ (mag)	$r'-i'$ (mag)	$i'-z'$ (mag)
18.215 ± 0.225	13.82 ± 0.01	0.43 ± 0.02	0.14 ± 0.02	-0.01 ± 0.02

The Sloan colors converted to BVRI using Smith et al. (2002) are $R = 18.02 \pm 0.01$ with $B - R = 1.00 \pm 0.02$, $V - R = 0.36 \pm 0.02$, and $R - I = 0.35 \pm 0.02$. The error on $m_{r'}$ is large because of the significant light curve while the error on $M_R(1, 1, 0)$ is shown to be much smaller as we use the mean of the light curve.

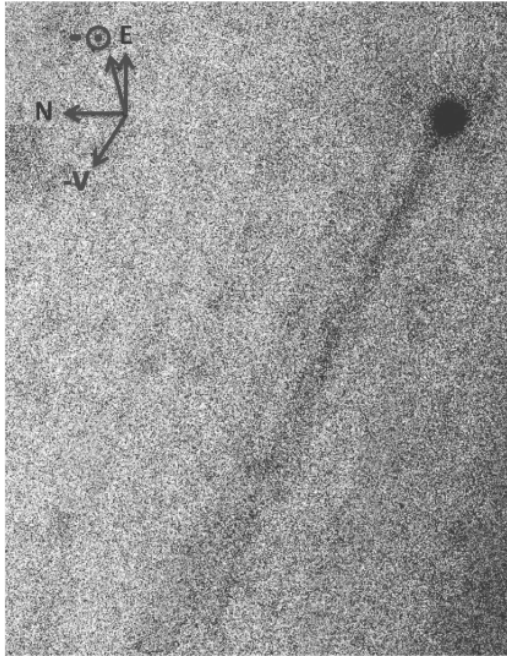


Fig. 1.— A 3750 second median exposure (Six 420 second VR filter and forty-one 30 second r' -band exposures) from IMACS on Magellan showing a tail for main belt object 62412. The image is about 1.7 arcminutes high and 1.4 arcminutes wide. East is up and North to the left. The antisolar direction ($-\odot$) and negative velocity vector ($-V$) are shown as projected on the sky. The observed tail is aligned with the negative velocity vector indicating large or slow moving particles in the orbital plane of 62412.

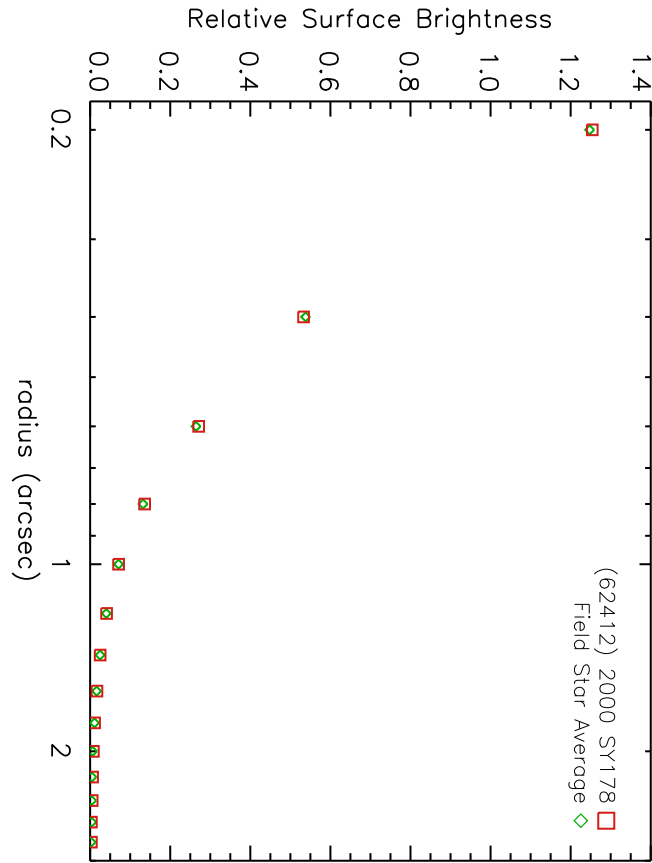


Fig. 2.— The relative surface brightness profile of 62412 (red squares) and the average of seven field stars (green diamonds) on the combined forty-one 30 second r' -band exposures from Magellan. There is no apparent extended brightness for 62412 compared to the field stars. This indicates 62412 has little to no coma surrounding the nucleus.

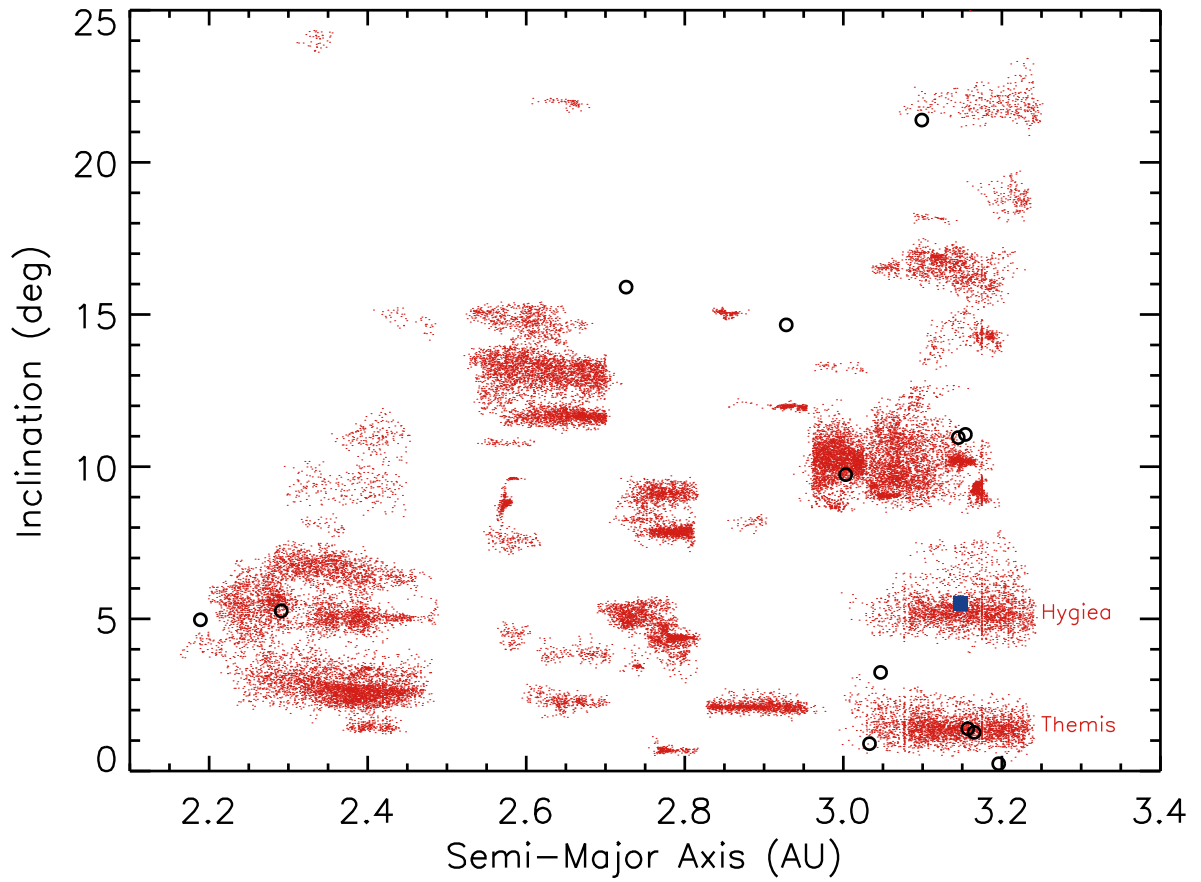


Fig. 3.— Semi-major axis versus inclination for known active asteroids (open circles), known asteroids in a family (red dots) and new active asteroid 62412 (solid blue square). 62412 is the first active asteroid known in the Hygiea family.

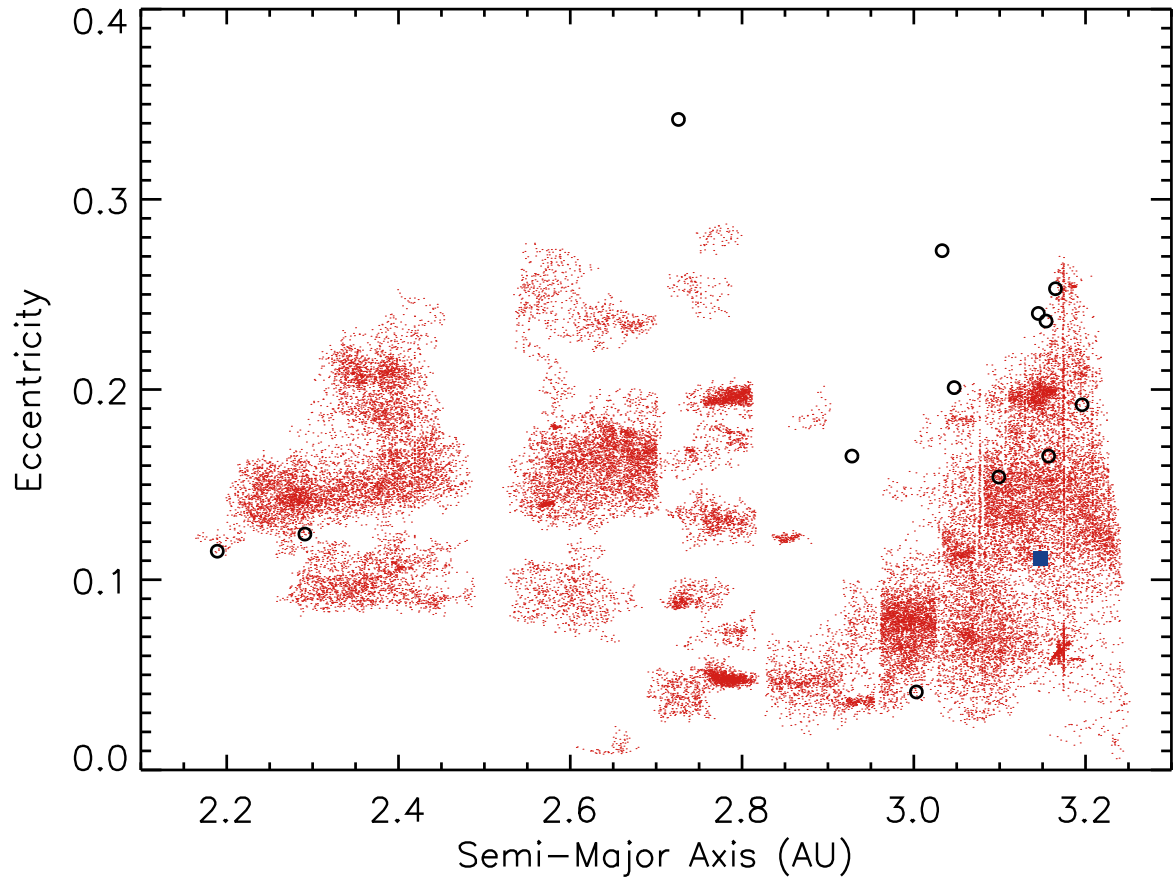


Fig. 4.— The semi-major axis versus eccentricity with symbols the same as Figure 3. 62412 has one of the lowest known eccentricities of an active asteroid, which is currently around 0.082 though its proper eccentricity averaged over 100 Myrs is shown here as 0.114 (see Table 3).

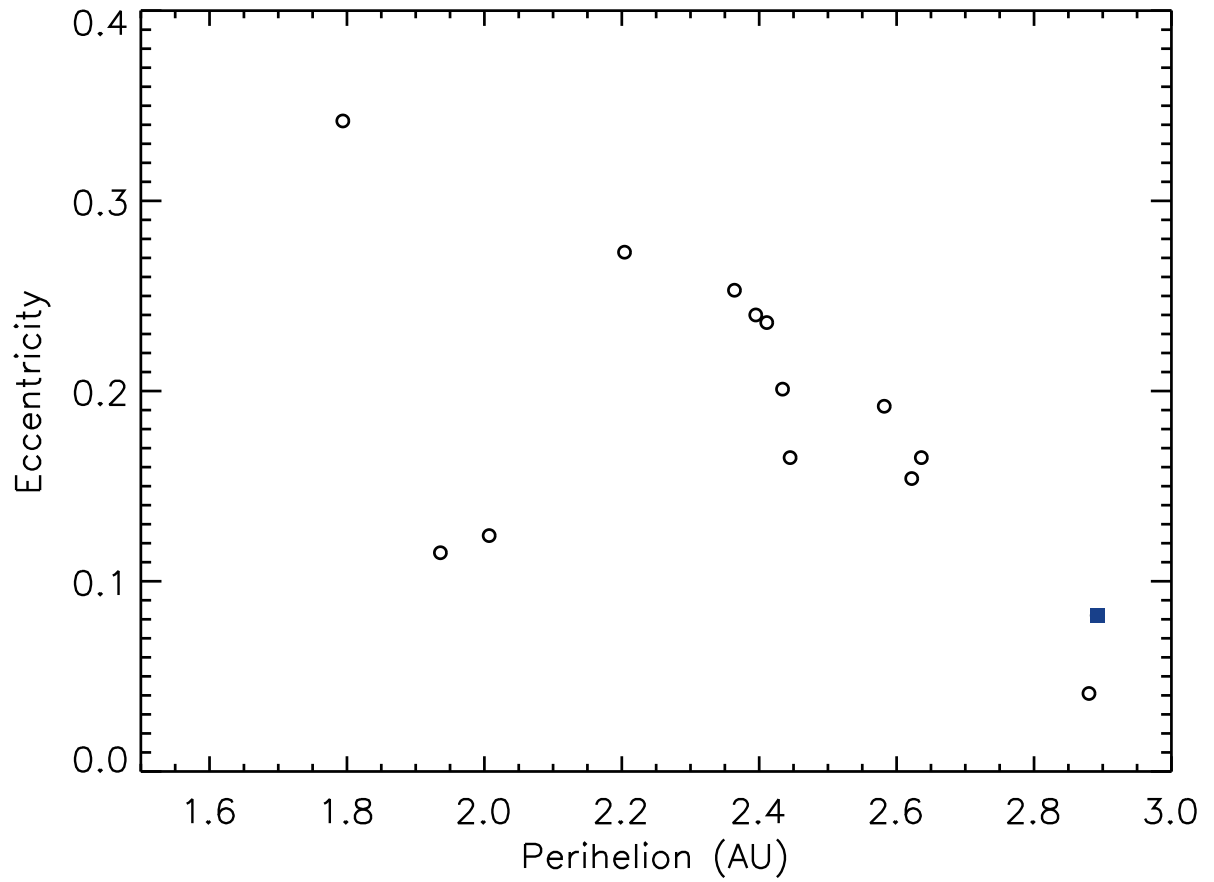


Fig. 5.— The perihelion versus eccentricity for known active asteroids. 62412 currently has the most distant perihelion and one of the lowest eccentricities of any known active asteroid.

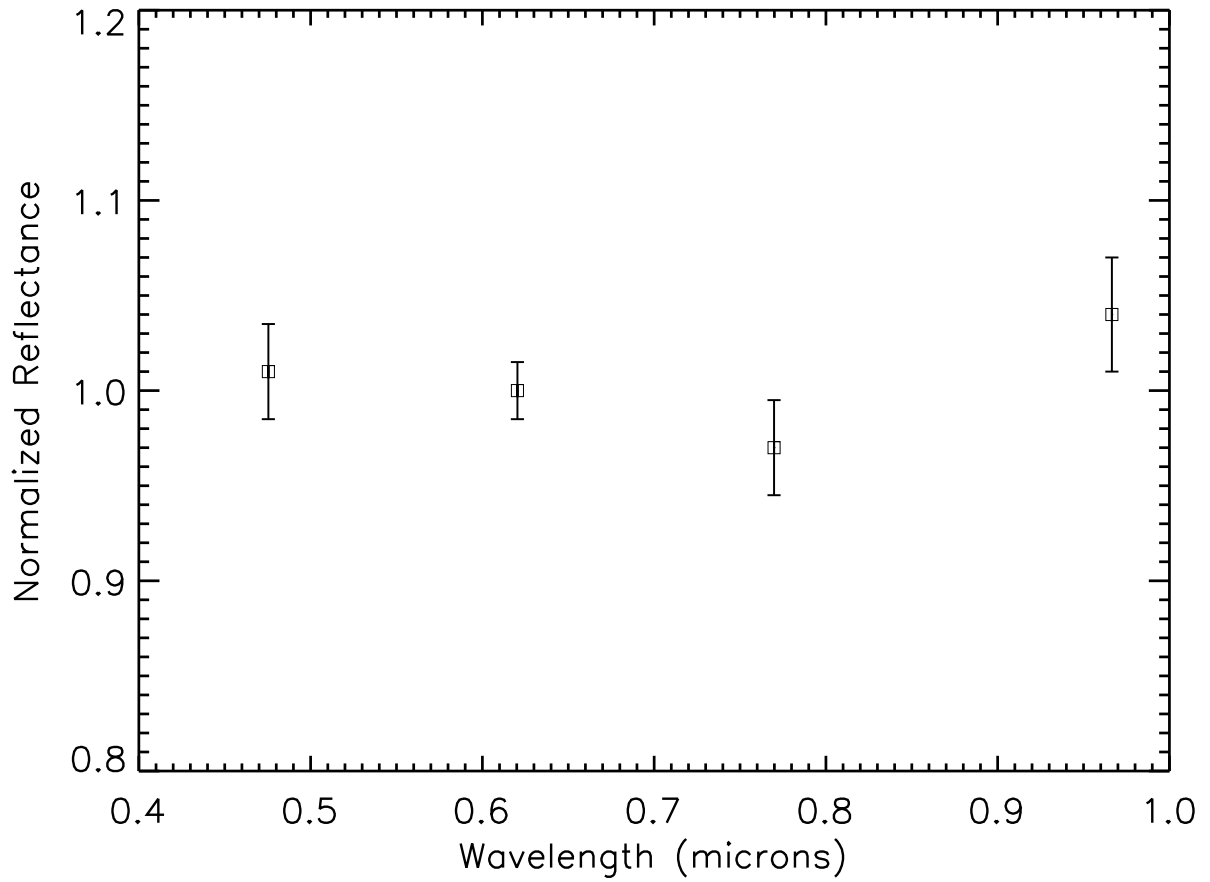


Fig. 6.— The normalized spectral slope of 62412 with the color of the Sun removed. Data are displayed at the central wavelengths of the g' , r' , i' , and z' Sloan broad-band filters. The flat spectrum is consistent with C-type asteroids.

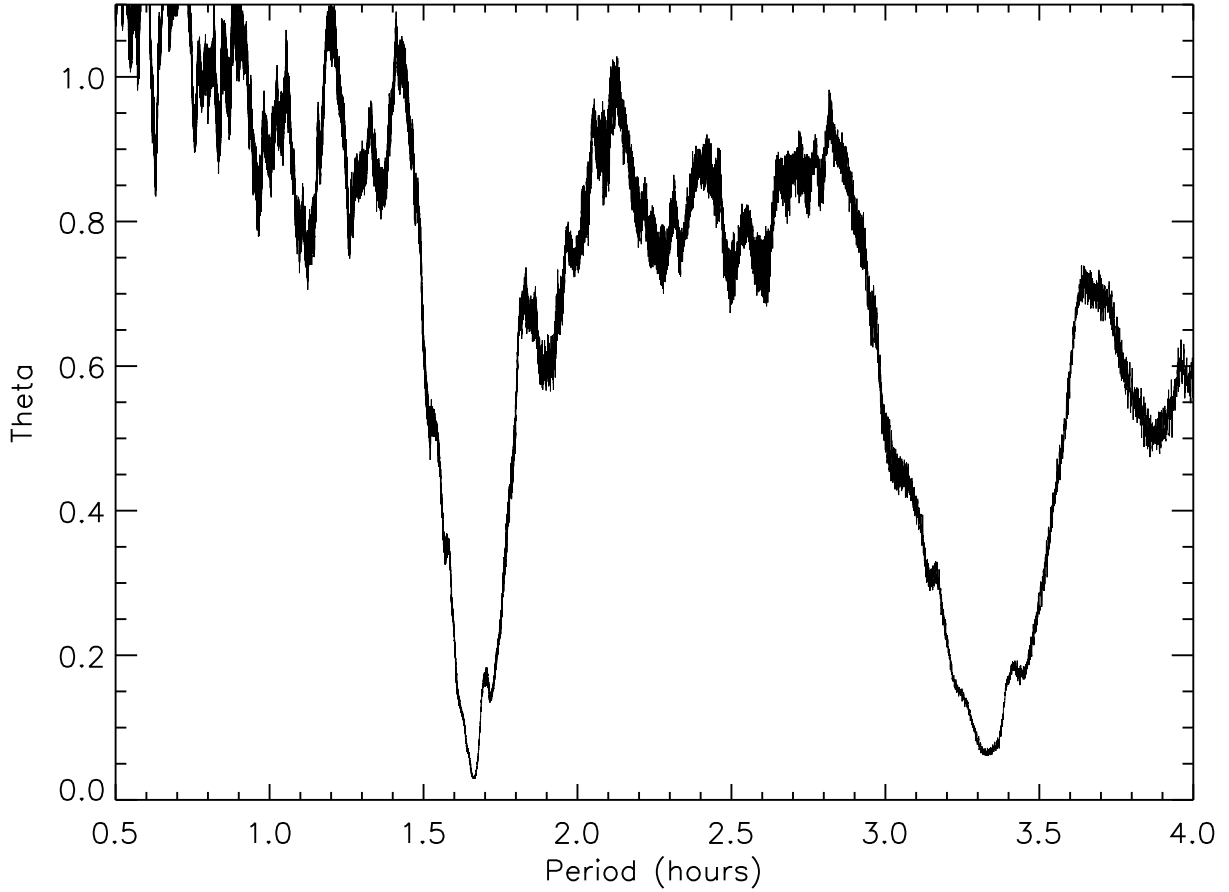


Fig. 7.— The Phase Dispersion Minimization (PDM) plot for 62412. The best fit single-peaked period is about 1.665 hours while the best fit double-peaked period is about 3.33 hours. Phasing the data together shows two distinct peaks and thus the double-peaked period at 3.33 hours is favored.

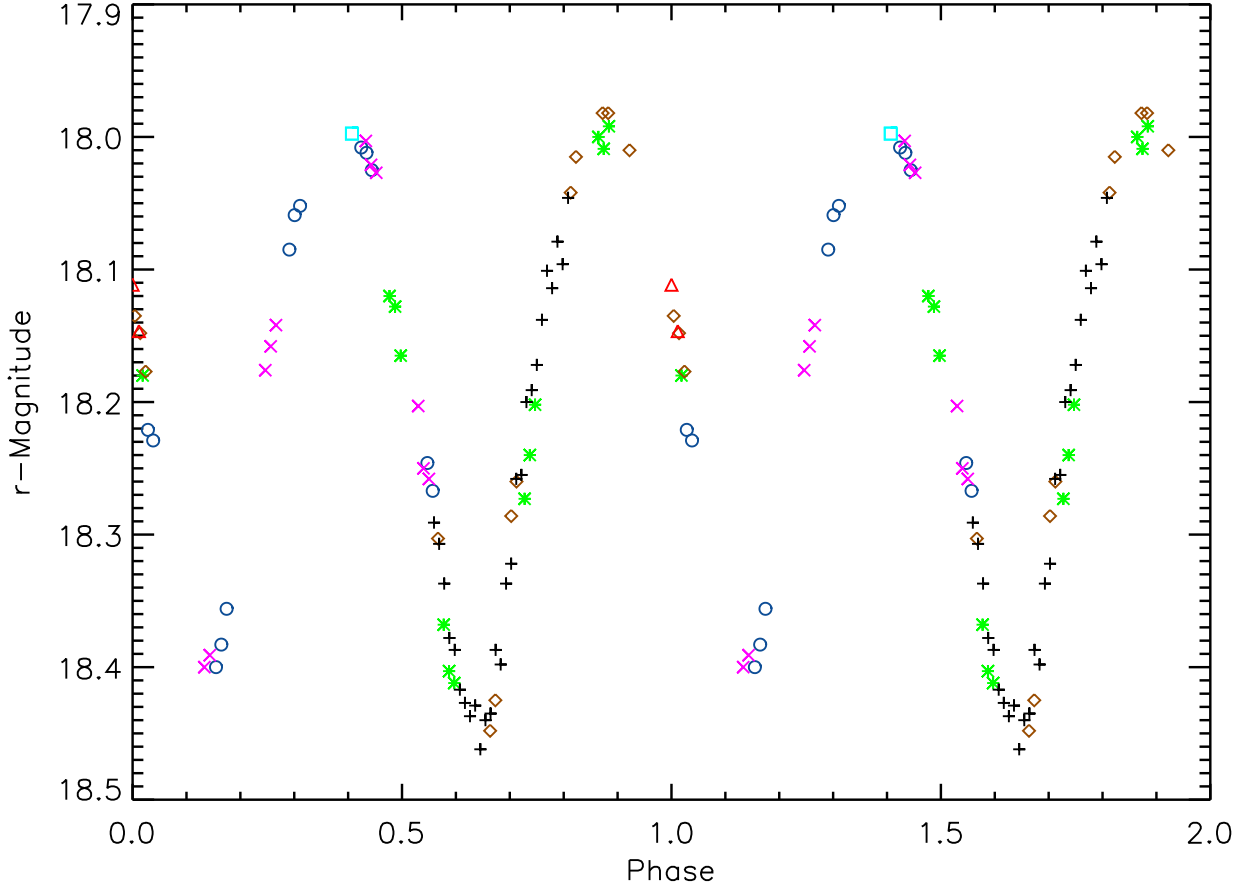


Fig. 8.— The phased best fit double-peaked period for 62412 of 3.33 hours. The maximum peak-to-peak amplitude is 0.45 ± 0.01 . The two lower peaks have a difference of about 0.05 magnitudes showing 62412 has an elongated irregular shape and a light curve dominated by shape rather than albedo effects. The red triangles are from May 1, 2014 while the rest of the symbols are from May 2, 2014 where the different symbols each represent distinct 1.66 hour time intervals (each half of the double-peaked light curve).

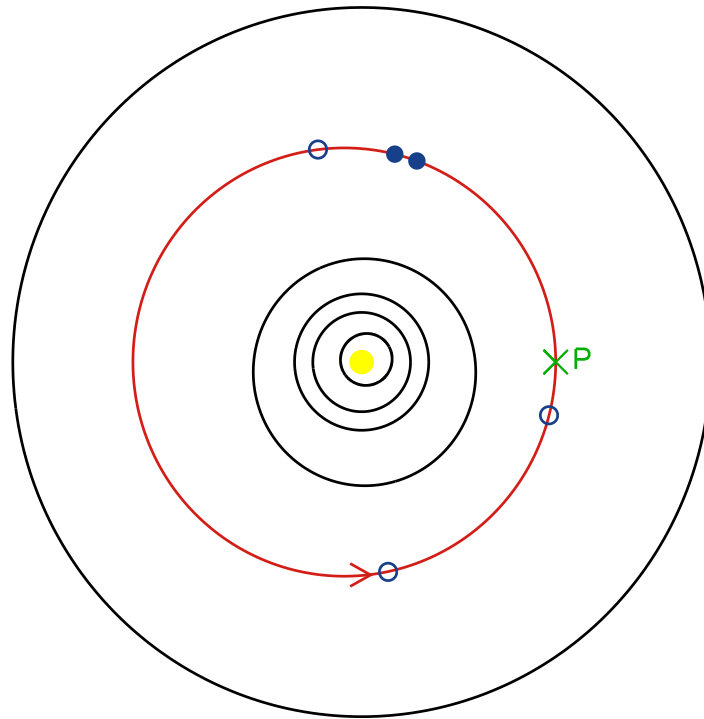


Fig. 9.— The orbit of 62412 (red) compared to the inner planets Mercury, Venus, Earth and Mars and the outer planet Jupiter (black). The perihelion of 62412 is shown by the green X and P while epochs of observations are shown by blue circles. Filled blue circles show where a tail was observed and open blue circles show where the tail was not observed near 62412.

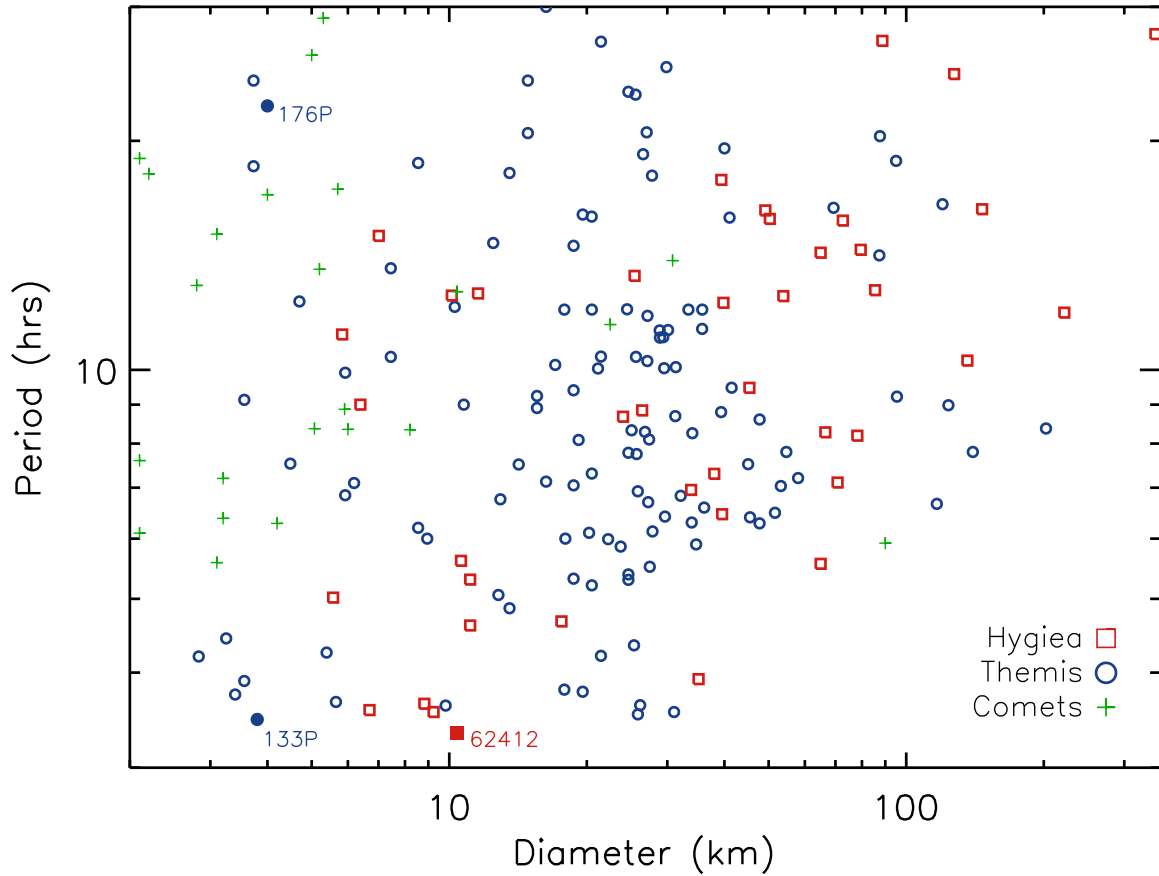


Fig. 10.— The size versus rotation period of asteroids in the Hygiea (red squares) and Themis (blue circles) asteroid families and short and long period comets (green pluses). 62412 has the fastest rotation of any member of these families (solid red square). Similarly, active asteroid 133P in the Themis family has the second known fastest period of any of these objects (solid blue circle). This strongly suggests rotation is important in producing the activity of these objects.

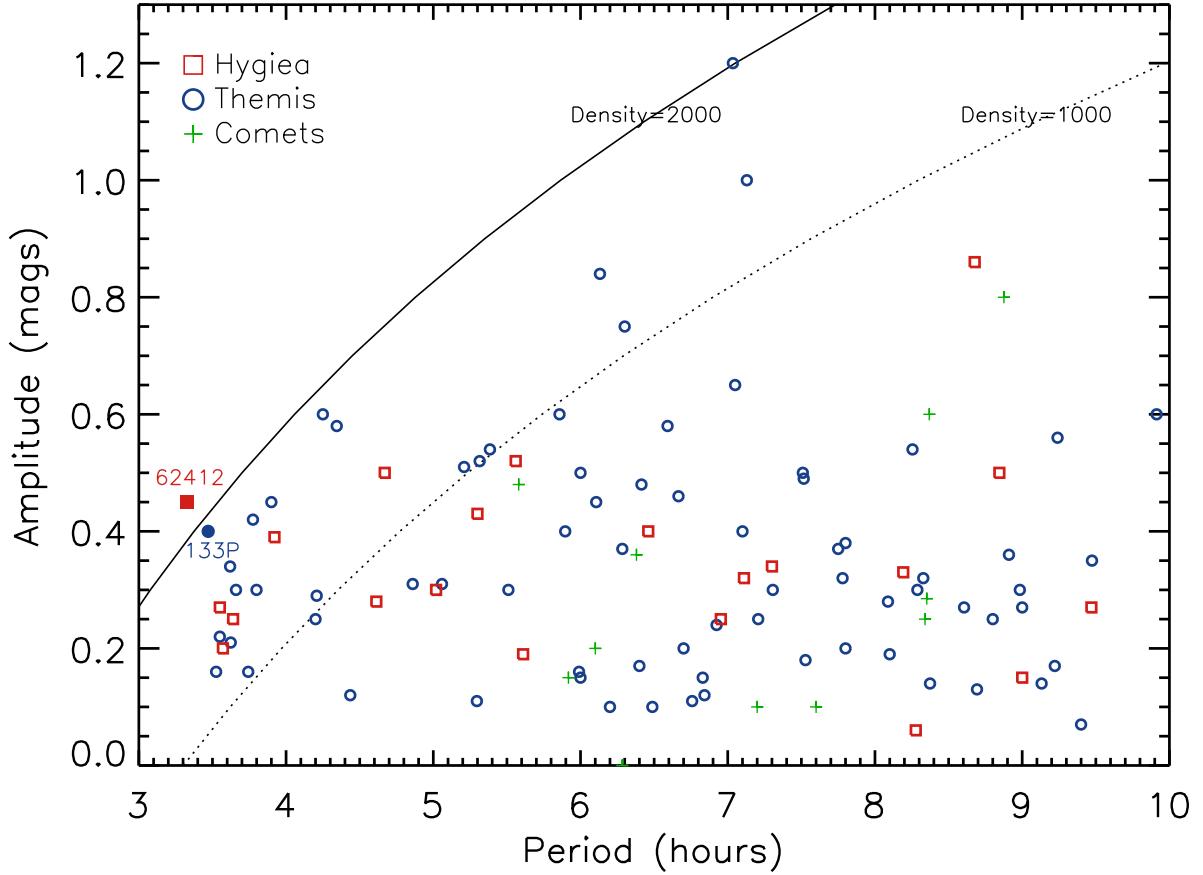


Fig. 11.— The periods versus the amplitudes of asteroids in the Hygiea (red squares) and Themis (blue circles) asteroid families and short and long period comets (green pluses). The critical period for densities of 1000 (dotted line) and 2000 (solid line) kg m^{-3} are shown using Equation 2. Objects to the left of these lines would need higher densities to be stable. As shown in the figure, 62412 would require the highest density to stay stable. Interestingly, asteroid (656) Beagle is near the density line of 2000 kg m^{-3} with a period of about 7 hours and amplitude of about 1.2 mags. Beagle is the largest member of a young ~ 10 Myr sub-family of the Themis population (Nesvorny et al. 2008).